

# Numerical Investigation of the Macroscopic Mechanical Behavior of NiTi-Hybrid Composites Subjected to Static Load–Unload–Reload Path

Fathollah Taheri-Behrooz and Ali Kiani

(Submitted November 6, 2016; in revised form January 29, 2017; published online February 23, 2017)

Shape memory alloys (SMAs) are a type of shape memory materials that recover large deformation and return to their primary shape by rising temperature. In the current research, the effect of embedding SMA wires on the macroscopic mechanical behavior of glass–epoxy composites is investigated through finite element simulations. A perfect interface between SMA wires and the host composite is assumed. Effects of various parameters such as SMA wires volume fraction, SMA wires pre-strain and temperature are investigated during loading–unloading and reloading steps by employing ANSYS software. In order to quantify the extent of induced compressive stress in the host composite and residual tensile stress in the SMA wires, a theoretical approach is presented. Finally, it was shown that smart structures fabricated using composite layers and pre-strained SMA wires exhibited overall stiffness reduction at both ambient and elevated temperatures which were increased by adding SMA volume fraction. Also, the induced compressive stress on the host composite was increased remarkably using 4% pre-strained SMA wires at elevated temperature. Results obtained by FE simulations were in good correlation with the rule of mixture predictions and available experimental data in the literature.

**Keywords** load–unload–reload, NiTi, polymer composites, thermomechanical

## 1. Introduction and Background

In recent years, the use of shape memory alloys due to their special properties such as shape memory effect, pseudoelasticity and high damping capability is increased in smart structures and actuators. Shape memory alloy hybrid composites (SMAHCs) are a type of smart structures that generally have higher strength, stiffness, fracture energy and natural frequency in comparison with unreinforced composites (Ref 1–6). Thus, these reinforced structures are interesting candidates for many applications in aerospace, biomechanics and civil engineering fields. The stress–strain behavior of these hybrid composites under mechanical loading is similar to a bilinear curve due to the martensitic transformation of embedded SMA wires. Shape recovery effect of SMA wire can lead to reduced matrix cracking and stress concentration at the tip of cracks in hybrid composites (Ref 7). Asadi et al. (Ref 8) analyzed the nonlinear behavior of thermal stability of the reinforced Timoshenko Beams with SMA. They used first-order theory and one-dimensional Brinson constitutive law for kinematic assumptions. Their findings express that the recovery stress caused by activation of SMA fiber can stabilize an imperfect beam subjected to heating. Deng et al. (Ref 9) investigated the mechanical behavior of uniaxial reinforced concrete specimen

with SMA wires. Also, the authors studied the effects of initial pre-strain, actuation time and temperature rising. According to the obtained experimental results, SMA wires can control the axial strain of specimens by activating and producing prestress. Applying pre-strain into SMA wires and using of SME capability at elevated temperature would cause a remarkable reversible force on the host composite. However, it should be noted that application of higher pre-strain values may lead to separation between the host composite and the SMA wires (Ref 10). Therefore, it is necessary to investigate the thermomechanical behavior of the polymeric composites reinforced with pre-strained SMA wires to optimize the mechanical performance. Many investigations have been performed on the macroscopic mechanical behavior of composites reinforced with SMA wires under different loading conditions and illustrated that the application of the shape memory wires can improve strength, stiffness and fracture energy of the host composite (Ref 11–16). Su et al. (Ref 11) presented a constitutive equation to simulate the thermomechanical behavior of composites reinforced with unidirectional SMA wires using irreversible thermodynamics. Also, they proposed a constitutive relation for modulus as a function of temperature to predict the stress–strain behavior of composites at different temperatures. Shimamoto et al. (Ref 12) investigated shape recovery effect of the SMA wires on the stress concentration of the crack tips using direct and indirect heating methods of the SMA wires. Lee and Taya (Ref 13) introduced a theoretical model, to predict yield stress of metal matrix composites integrated with SMA wires. According to the obtained results, yield stress in composites for pre-strain values between zero and 2% was increased, while for the values between 2 and 3% was decreased or remained constant. Damanpack et al. (Ref 14) investigated the thermomechanical response of metal matrix composites reinforced with SMA wires under multi-axial proportional and non-proportional loading. According to their

Fathollah Taheri-Behrooz and Ali Kiani, School of Mechanical Engineering, Iran University of Science and Technology, P.O.B. 1684613114, Tehran, Iran. Contact e-mails: taheri@iust.ac.ir and a.k.alikiani@gmail.com.

observations, by increasing the pre-strain value for SMA wires, the recovery stress was increased. Also, they found that martensitic transformation of SMA fiber and plastic deformation of the aluminum matrix are inducing a plateau with the low slope in the stress–strain curve. Zhu and Dui (Ref 15) presented a micromechanical model to simulate mechanical behavior of aluminum matrix reinforced with shape memory alloys. The effect of three shapes of SMA inclusions as short fiber, long fiber and the spherical particle was investigated on the overall mechanical behavior of the SMAH composite. They found that the overall stiffness of the hybrid composites containing the long fibers was the maximum, while the residual strains of the hybrid composites containing the spherical particles were more than the others. Raghavan et al. (Ref 16) investigated the ability of SMA wires to improve damping, tensile and impact properties of SMAH's. Lei et al. (Ref 17) studied the effect of adding short SMA wires on thermomechanical behavior of composites. According to their findings, increasing SMA volume fraction would increase composite Young's modulus and vice versa. Lei et al. (Ref 18) studied the effect of the interface on macroscopic behavior of shape memory alloy hybrid composites. They reported a bilinear curve for hybrid composites due to the martensitic transformation of SMA wires with 3.4% improvement in ultimate tensile strength. Also, they point out that ultimate strength is limited by the weak interface of hybrid composite. Taheri et al. (Ref 4) experimentally investigated the thermomechanical behavior of reinforced composites with pre-strained SMA wires under static loading at different temperatures. They assumed perfect interfacial bonding between the SMA fiber and matrix in their research. They performed a tensile test on the hybrid composite specimens and showed that application of SMA fibers at elevated temperature could improve the overall structural response of the host composite in terms of stiffness and strength.

The objective of the present article is to investigate the thermomechanical behavior of shape memory alloy hybrid composites (SMAHCs) by assuming perfect interface between SMA fiber and the host composite. In this study, SMAHCs are simulated using Ansys software and the effect of different parameters such as wires volume fraction, activation temperature and pre-strain is investigated on their thermomechanical response. In addition, mechanical behavior of these materials under loading–unloading and reloading conditions at both room and elevated temperatures is investigated for the first time. In order to quantify the extent of the induced compressive stress in the host composite and the residual tensile stress in the SMA wires, a theoretical modeling approach is introduced based on the one-dimensional material model of SMA wires. Results of the finite element simulations are compared with the available experimental data in the literature.

### 1.1 Constitutive Equations

So far, many constitutive equations with various capabilities are introduced to predict the thermomechanical behavior of SMA wires. The related one-dimensional and three-dimensional equations could be found in (Ref 19-22) and (Ref 23-25), respectively. In this article, the one-dimensional Brinson's model is utilized. In this theory, internal variable martensite volume fraction for the first time was decomposed to stress and temperature components.  $\xi_T$  and  $\xi_S$  represent temperature and stress-induced martensite volume fractions, respectively.

According to this constitutive equation, the martensite volume fraction and stress is as follows:

$$\xi = \xi_T + \xi_S \quad (\text{Eq 1})$$

$$\sigma - \sigma_0 = E(\xi)\varepsilon - E(\xi_0)\varepsilon_0 + \Omega(\xi)\xi_S - \Omega(\xi_0)\xi_0 + \Theta(T - T_0) \quad (\text{Eq 2})$$

The subscript 0 refers to the initial reference state. Symbols  $E$ ,  $\Omega$ ,  $\xi$  and  $\Theta$  represent the elastic modulus, phase transformation modulus, martensite volume fraction and thermoelastic tensor, respectively. In this model, the overall modulus is assumed as a linear function of the modulus of austenite and martensite phases as shown below:

$$E(\xi) = E_s^a + (E_s^m - E_s^a)\xi \quad (\text{Eq 3})$$

where  $E_s^a$  and  $E_s^m$  are the austenite and martensite phase modulus. According to  $E(\xi)$ , other modules are assumed as a linear function of  $\xi$  and expressed as:

$$\Omega(\xi) = -\varepsilon_L E(\xi) \quad (\text{Eq 4})$$

$$\Theta(\xi) = E(\xi)(\alpha_a + (\alpha_m - \alpha_a)\xi) \quad (\text{Eq 5})$$

where  $\varepsilon_L$  is the maximum residual strain and  $\alpha_a$  and  $\alpha_m$  are the thermal expansion coefficients in austenite and martensite phases, respectively.

The evolution equations for martensite volume fraction ( $\xi$ ) in forward transformation (austenite to martensite phase) and reverse transformation (martensite to austenite phase) are expressed as:

From austenite into martensite phase:

$$\sigma_s^{\text{cr}} + C_M(T - M_s) < \sigma < \sigma_f^{\text{cr}} + C_M(T - M_s) \quad \text{and} \quad T > M_s \quad (\text{Eq 6})$$

$$\xi_S = \frac{1 - \xi_{S0}}{2} \cos \left[ \frac{\pi}{\sigma_s^{\text{cr}} - \sigma_f^{\text{cr}}} \{ \sigma - \sigma_f^{\text{cr}} - C_M(T - M_s) \} \right] + \frac{1 + \xi_{S0}}{2} \quad (\text{Eq 7})$$

For  $T < M_s$  and  $\sigma_s^{\text{cr}} < \sigma < \sigma_f^{\text{cr}}$

$$\xi_S = \frac{1 - \xi_{S0}}{2} \cos \left[ \frac{\pi}{\sigma_s^{\text{cr}} - \sigma_f^{\text{cr}}} \{ \sigma - \sigma_f^{\text{cr}} \} \right] + \frac{1 + \xi_{S0}}{2} \quad (\text{Eq 8})$$

From martensite into austenite phase:

$$C_A(T - A_f) < \sigma < C_A(T - A_s) \quad \text{and} \quad T > A_s \quad (\text{Eq 9})$$

$$\xi_S = \frac{1 - \xi_{S0}}{2} \cos \left[ \frac{\pi}{\sigma_s^{\text{cr}} - \sigma_f^{\text{cr}}} \{ \sigma - \sigma_f^{\text{cr}} - C_M(T - M_s) \} \right] + \frac{1 + \xi_{S0}}{2} \quad (\text{Eq 10})$$

where  $C_A$  and  $C_M$  are the material constants to express the relationship between critical stress of phase transformation and temperature and  $A_s$ ,  $A_f$ ,  $M_s$ ,  $M_f$  are the start and finish temperatures in austenite and martensite transformations and symbols  $\sigma_s^{\text{cr}}$ ,  $\sigma_f^{\text{cr}}$ ,  $T$ ,  $\xi_s$ ,  $\xi_{s0}$  refer to the critical stress at the start and finish of the martensite transformation, temperature, martensite volume fraction induced by stress and initial martensite volume fraction, respectively.

### 1.2 Effective Modulus of SMAHC

Embedding SMA wires into the laminated composites lead to a change in mechanical properties such as stiffness, strength,

toughness and absorbed energy. In order to calculate effective modulus, the role of mixture relationship (ROM) is used. It should be noted that this law is valid for linear systems. In this study, the ROM on the initial linear part of SMA stress–strain curve and linear part of phase transformation is used separately. According to the ROM, effective modulus of SMAHC is given by:

$$E_{\text{SMAHC}} = E_s V_s + E_m V_m + E_c V_c \quad (\text{Eq 11})$$

where  $E_s$ ,  $V_s$ ,  $E_c$ ,  $V_c$  and  $E_m$ ,  $V_m$  are the elastic modulus and volume fraction of SMA wire, composite and resin between SMA wire and composite layers, respectively. It should be noted that due to inserting a layer of SMA wire and resin inside prepreg composite layers, the resin volume fraction deposited between SMA wires is considered in all equations. Resin modulus is considered to be 2 GPa (Ref 4) at both room and elevated temperatures. By substituting Eq 3 into Eq 11, the elastic modulus of SMAHC is obtained as a function of martensite volume fraction:

$$E_{\text{SMAHC}} = V_s (E_s^a + (E_s^m - E_s^a) \xi) + E_m V_m + E_c V_c \quad (\text{Eq 12})$$

According to the ROM, the ultimate strength of SMAHC can be obtained from the following equation:

$$\sigma_{\text{SMAHC}}^u = V_s \sigma_s^u (\varepsilon_{\text{max}}^s) + V_{\text{comp}} \sigma_{\text{comp}}^u (\varepsilon_{\text{max}}^{\text{comp}}) \quad (\text{Eq 13})$$

where  $\sigma_s^u$  and  $\sigma_c^u$  are the ultimate strength of SMA wire and SMAHC, respectively.

### 1.3 Compressive Initial Stress Induced in the Host Composite

Based on the experiments performed by Taheri et al. (Ref 4), SMAHC specimens are fabricated as shown in Fig. 1. Initially, SMA wires are wrapped around on a metallic frame and strained up to 4% of their initial length. In the second step, six

layers of E-glass/epoxy prepreps are laid below and on the SMA wires to construct SMAHC plates as [(E-glass/epoxy)<sub>3</sub>/SMA layer/(E-glass/epoxy)<sub>3</sub>]. At the final step, curing of the SMAHC plate is completed and then SMA wires are released from the frame to compress the host composite.

This manufacturing process extended induced compressive strain ( $\varepsilon_c$ ) in the host composite. The total strain in SMA wires consists of elastic strain and phase transformation strain. By unloading a pre-strained SMA wire, the elastic strain part will be recovered but the other part will be remained as residual strain. A typical stress–strain relationship of SMA wire is shown in Fig. 2.

Therefore, total strain in SMA wire is expressed as:

$$\bar{\varepsilon}_{\text{total}} = \bar{\varepsilon}_{\text{lin}} + \bar{\varepsilon}_{\text{res}} \quad (\text{Eq 14})$$

where  $\bar{\varepsilon}_{\text{lin}}$  and  $\bar{\varepsilon}_{\text{res}}$  denote the elastic and residual strains, respectively. After embedding SMA wire in composite and then releasing them, the composite will stunt the returning of SMA wires. After releasing SMA wires, a part of the elastic strain of the SMA wires remained in the wires ( $\varepsilon_r$ ) and the other part recovered ( $\varepsilon_{\text{rec}}$ ), so one may write:

$$\bar{\varepsilon}_{\text{lin}} = \varepsilon_{\text{rec}} + \varepsilon_r \quad (\text{Eq 15})$$

Assuming the perfect interfacial bonding between the SMA wires and the composite matrix, all recovered part of the strain induced to the composite matrix, which means:

$$\varepsilon_{\text{rec}} = \|\varepsilon_c\| \quad (\text{Eq 16})$$

where  $\|\varepsilon_c\|$  is the magnitude of the compressive strain in the composite. Substituting Eq 16 into Eq 15, the elastic strain of the SMA wires is obtained as follows:

$$\bar{\varepsilon}_{\text{lin}} = \varepsilon_c + \varepsilon_r \quad (\text{Eq 17})$$

Due to the perfect interfacial bonding assumption, the action and reaction forces created between the SMA wires and the host

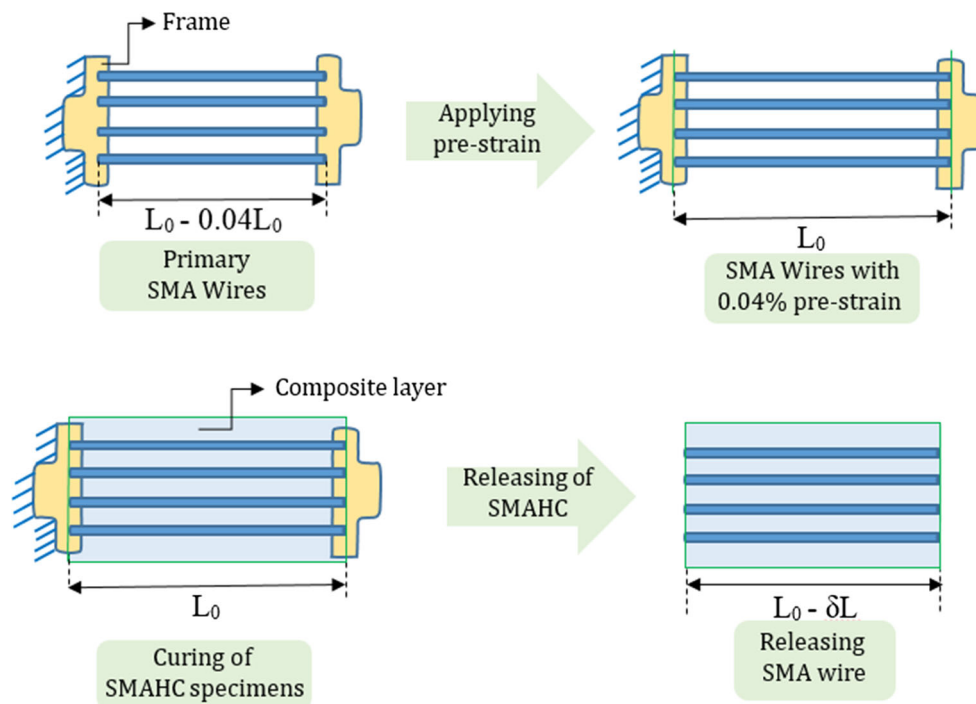


Fig. 1 Schematic of embedding pre-strained SMA wires in the host composite

composite are considered equal. The elastic strain of SMA wire is expressed as follows (Ref 19):

$$\varepsilon_f = \sigma_{SMA} / E_{SMA} = f / A_{SMA} E_{SMA} \quad (\text{Eq 18})$$

where  $E_{SMA}$  is the elastic modulus of SMA wires in the return path at 4% strain and  $f$  is the equivalent force between SMA wires and matrix. By considering linear and similar properties in the longitudinal and transverse directions for the host composite, one may write:

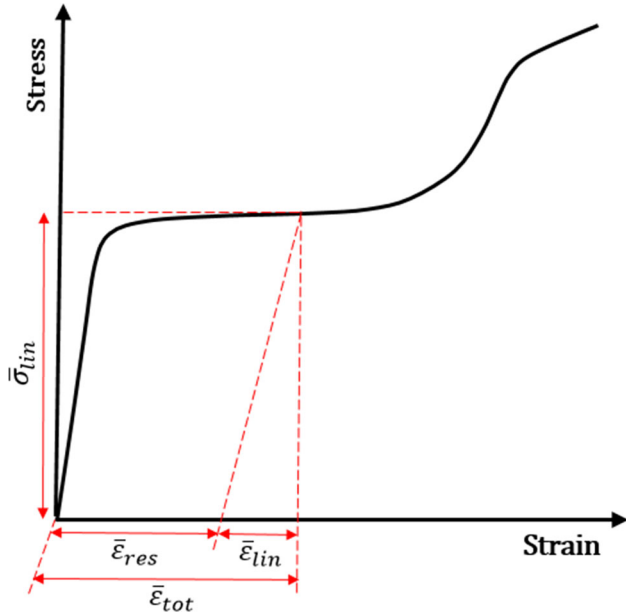


Fig. 2 Schematic of stress–strain relationship of SMA wire

$$\varepsilon_c = \sigma_c / E_c = f / A_c E_c \quad (\text{Eq 19})$$

$$E_c = V_{PC} E_{PC} + V_m E_m \quad (\text{Eq 20})$$

where  $V_{PC}$ ,  $V_m$  is the volume fraction of initial composite (prepreg composite) and matrix between SMA wires and composite, respectively. By substituting Eq 18 and Eq 19 into Eq 17, the  $f$  force is obtained as follows:

$$f = \frac{\bar{\varepsilon}_{lin}}{\left( \frac{1}{A_c E_c} + \frac{1}{A_{SMA} E_{SMA}} \right)} \quad (\text{Eq 21})$$

Using obtained equivalent force ( $f$ ) and Eq 19, initial compressive stress into the host composite is obtained as follows and illustrated in Table 1.

$$\sigma_c = E_c \varepsilon_c = \frac{\bar{\varepsilon}_{lin}}{\left( \frac{1}{E_c} + \frac{A_c}{A_{SMA} E_{SMA}} \right)} \quad (\text{Eq 22})$$

## 2. Properties of SMAHC Constituents

SMAHC specimens consist of composite matrix and SMA wires with various volume fractions of the constituents. Constituents mechanical properties based on the experiments performed by the other researchers are illustrated in Table 2 (Ref 4, 26, 31). The composite matrix is made of impregnated woven E-glass/epoxy layers, and its properties at ambient (26 °C) and elevated (90–100 °C) temperatures are obtained from (Ref 4, 26). According to (Ref 4), for these woven E-glass/epoxy materials the same mechanical properties are

Table 1 Amount of induced stress and strain in the host composite and SMA wires after releasing the SMA wires

Percentage	Temp	$E_c$ , GPa	$E_{SMA}$ , GPa	$f$ , N	$\bar{\varepsilon}_{lin} \times 10^3$	$\varepsilon_f \times 10^3$	$\varepsilon_c \times 10^3$	$\sigma_c$ , MPa	$\sigma_s$ , MPa
4% SMA and 11.86% resin	Ambient	20.43	28	362.4	7.5	7.095	0.405	−8.27	198.7
	Elevated	20.43	53.78	1692.8	19.15	17.26	1.893	−38.67	928.1
7% SMA and 8.86% resin	Ambient	20.37	28	607.5	7.5	6.80	0.703	−14.32	190.3
	Elevated	20.37	53.78	2742.4	19.15	15.98	3.175	−64.67	859.2
10% SMA and 5.86% resin	Ambient	20.31	28	830.4	7.5	6.50	0.996	−20.23	182.1
	Elevated	20.31	53.78	3628.7	19.15	14.80	4.35	−88.42	795.8

Table 2 Material properties of the host composite and the SMA wires at ambient and elevated temperatures (Ref 4, 26, 31)

E11, GPa	E22, GPa	E33, GPa	Strength, MPa	$K_{xy}$	$K_{xz} = K_{yz}$	$G_{xy}$ , GPa	$G_{xz} = G_{yz}$ , GPa
<i>Composite</i>							
24	24	5.14	540	0.138	0.3	4.2	2.57
$E_a$ , GPa	$E_m$ , GPa	$\bar{\varepsilon}_L$	$\beta$ , MPa/°C	$R$ , MPa	$T_0$ , k	$h$ , MPa	$T_{as}$ , °C
<i>SMA wires</i>							
80	28	0.0675	13.65	160	325.15	500	69
$T_{ab}$ , °C	$T_{ms}$ , °C	$T_{mf}$ , °C	$C_M$ , MPa/°C	$C_A$ , MPa/°C	$\sigma_s^{cr}$ , MPa	$\sigma_f^{cr}$ , MPa	K
<i>SMA wires</i>							
84	52	42	8.44	13.65	187	225	0.33

obtained at elevated and the ambient temperatures. Also according to (Ref 4), the NiTi SMA wires used was obtained by Memry Corp. (Bethel, CT), composed of nickel and titanium (as are most of the commercial NiTiNOL wires); the diameter of the SMA wire was 0.381 mm. Thermomechanical properties of the SMA wires at room and elevated temperatures are tabulated in Table 2 (Ref 4, 31).

Symbols used in Table 2 are defined as follows.  $E_a, E_m, h, R, \beta, \bar{\epsilon}_L, \vartheta, T_0$  refer to austenite modulus, martensite modulus, hardening parameter during the phase transformation, elastic limit, temperature scaling parameter, maximum transformation strain, Poisson's ratio and the reference temperature, and symbols  $T_{as}, T_{af}, T_{ms}, T_{mf}$  refer to austenite start, austenite finish, martensite start and martensite finish temperatures, respectively.

### 3. Numerical Simulations Using ANSYS

In this section, a 3-D finite element simulation is performed according to the dimension of SMAHC specimens as the length of 220 mm, the width of 19 mm and thickness of 2.4 mm. For modeling the SMA wires, unidirectional solid cylinders along the axial direction of loading are embedded between layers of composites as a unidirectional layer. Due to the specimen symmetry, half of the plate is considered for the analysis. The SMA wires along with their surrounding matrix are considered as a single layer to construct the SMAHC laminate as [(E-glass/epoxy)<sub>3</sub>/SMA layer/(E-glass/epoxy)<sub>3</sub>]. According to the experiments performed by (Ref 4), the total volume fraction of SMA layers (SMA wire and its surrounded resin) and the host composite layers were 15.8 and 84.2%, respectively. The volume fraction of SMA wire in SMAHC sheet could be altered by changing SMA wires number and diameter in the middle layer of SMAHC sheet. As mentioned "SMA layer" is a combination of SMA wires and their surrounded resin with different percents which are explained in Table 1. Dimensions and boundary conditions used in FE modeling of SMAHC sheets are schematically shown in Fig. 3.

The simulation of SMA wires was conducted using Aurichio and Zouain (Ref 27-30) nonlinear models available in ANSYS material library. For simulation of SMA wires, brick elements (solid 185) are used and face sheets are modeled by using the same elements in Ansys software.

As shown in Fig. 3, the left edge of the model is fixed and a uniform load is applied along the right edge of the SMAHC along the axial direction of SMA wires. Since half of the specimen is simulated, the boundary condition of the upper edge is simply supported and the lower edge is free. The mesh convergence analysis is performed on a various number of elements to ensure the accuracy of calculations and freedom of

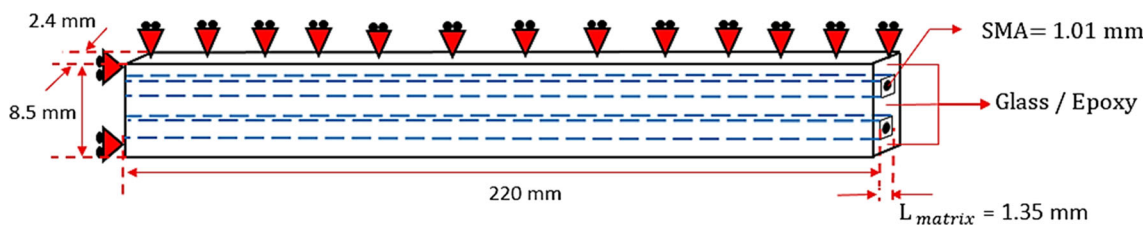


Fig. 3 Dimensions and boundary conditions used in FE modeling of SMAHC sheets

the model to mesh size. The final mesh distributions in thickness and around the SMA wire are shown in Fig. 4. The dimensions of elements in thickness, width and length directions are considered as 0.086, 0.084-0.148 and 1.375 mm, respectively. The number of brick elements used in final FE model for SMA wires surrounded resin and composite faces is 123,520, 61,440 and 122,880, respectively. Also, the minimum time step used in solution was  $10^{-4}$  (s) and nonlinear Newton-Raphson method was used during solution.

#### 3.1 Validation of the Numerical Simulations

Using properties of Table 2, the thermomechanical behavior of SMA wires at both temperatures is simulated and illustrated in Fig. 5. As depicted in Fig. 5, the results predicted by finite element simulation have good agreement with experimental results.

Predicted results of the FE simulation of SMAHC plates under static tensile loading are compared with experimental data obtained by (Ref 4), as well as with ROM predictions. Figure 6 shows the comparison between the results of the simulation and test results at ambient temperature. As depicted in Fig. 6, the global stress-strain behavior of the SMAHC plates is bilinear due to martensitic phase transformation of SMA wires.

As seen, deviation of FEM and ROM (Eq 12) predictions from the experiment started around 0.36% strain. This difference is mainly due to three possible reasons: (a) perfect bonding assumption of the interface in FE modeling, (b) numerical errors of FE simulation and (c) stiffness degradation due to micro-matrix cracking which is not simulated in FE simulation.

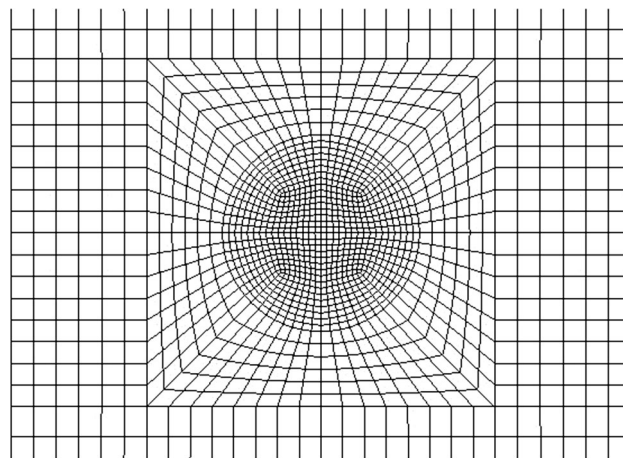


Fig. 4 Mesh distribution in thickness and around the SMA wire

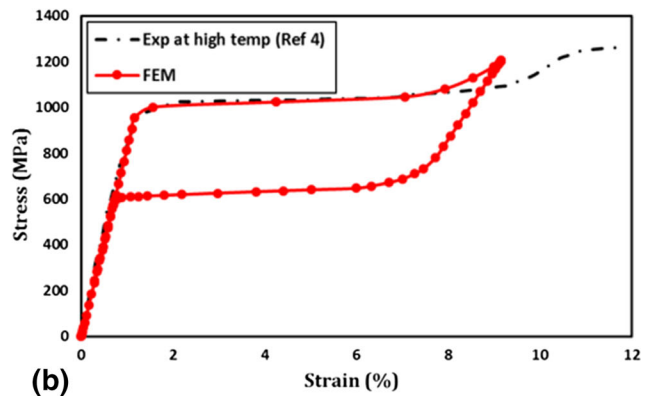
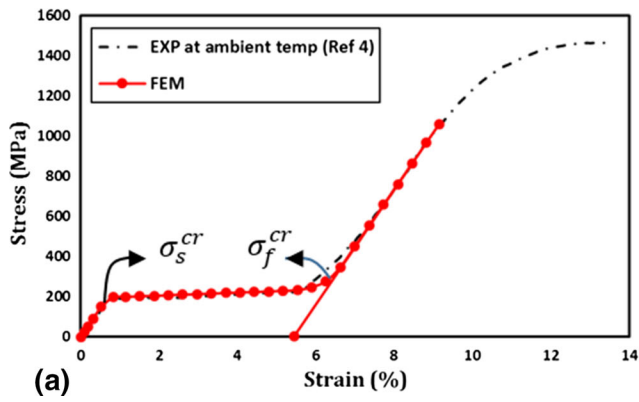


Fig. 5 Thermomechanical behavior of SMA wires at (a) ambient temp (left) and (b) elevated temp (right)

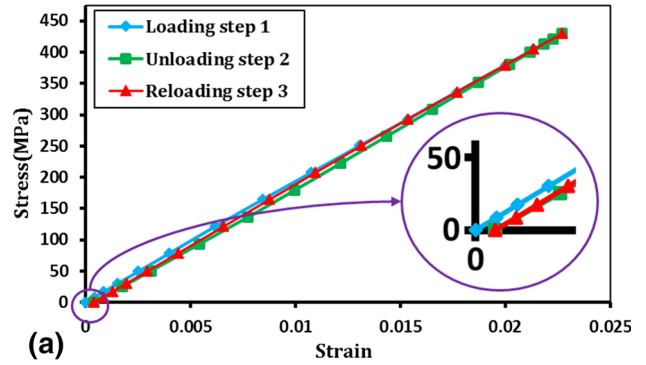
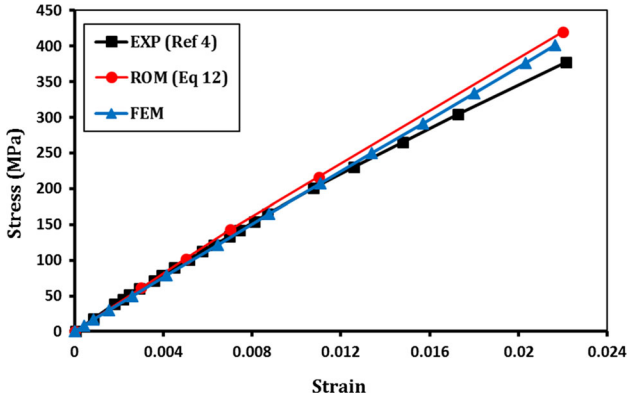


Fig. 6 Average stress–strain behavior of SMAHCs with 7% SMA wires at ambient temperature

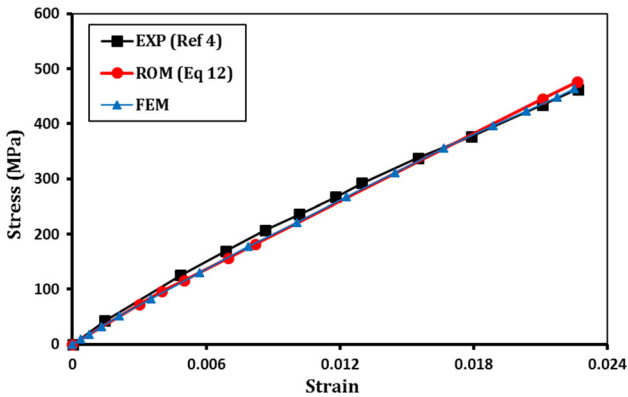


Fig. 7 Average stress–strain behavior of SMAHCs with 7% SMA wires at elevated temperature

As illustrated in Fig. 7, a good correlation between predicted results by FE simulation, experiment and ROM is obtained for the SMAHCs at elevated temperatures.

According to the results presented above, the general error of simulation at ambient and elevated temperatures in comparison with experimental results is less than 5.85, and 5.7%, respectively. In the following sections, the effect of various parameters on the global stress–strain behavior of SMAHC laminates will be studied numerically.

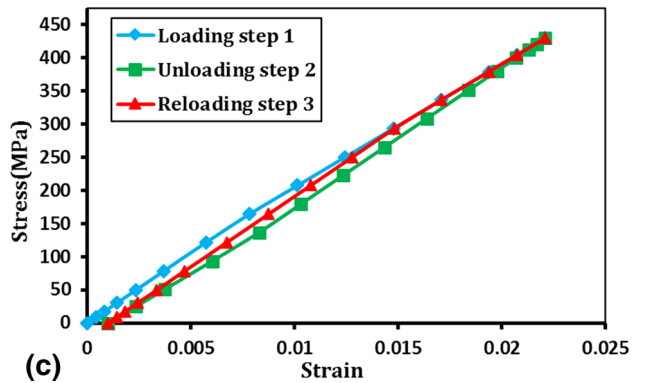
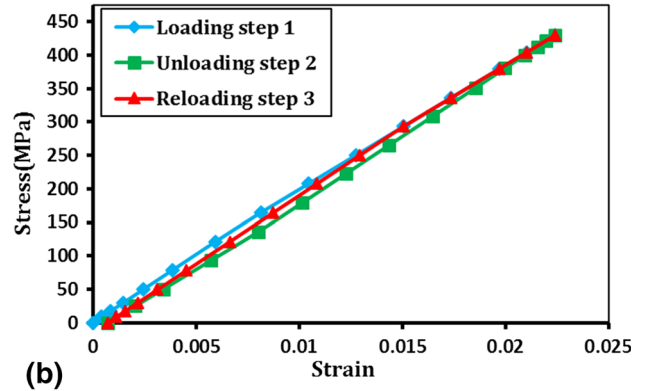
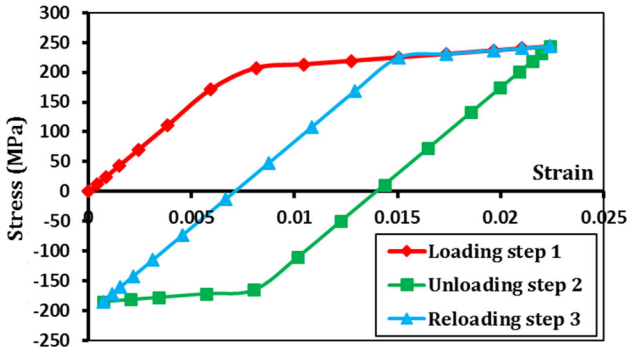


Fig. 8 Average stress–strain behavior of SMAHCs at ambient temperature, containing SMA wires with volume fractions of (a) 4%, (b) 7% and (c) 10%

**Table 3** Effects of SMA volume fraction on the effective modulus of SMAHCs containing SMA wires without pre-strained

SMA volume fraction	First stage			Second stage		
	4%	7%	10%	4%	7%	10%
Effective modulus, GPa						
Ambient temperature						
FEM	21.61	22.39	23.20	20.58	20.55	20.54
ROM (Eq 12)	21.55	22.33	23.11	20.47	20.44	20.41
Elevated temperature						
FEM	23.67	26.01	28.36	20.59	20.57	20.55
ROM (Eq 12)	23.63	25.97	28.31	20.47	20.44	20.41



**Fig. 9** Stress–strain response of SMA wire inside the SMAHC laminate at ambient temperature

### 3.2 Parametric Studies

It is well known that in two phase's materials that the volume fractions of the constituents play an important role in many characteristics of the final structure as in mechanical and thermal properties. In this section, the effect of different parameters of the reinforcement such as wires volume fraction, pre-strain and temperature is investigated on the stress–strain behavior of SMAHCs. Also, the effect of loading–unloading–reloading conditions on the amount of the induced residual stresses and strains on the host composite and SMA wires is evaluated.

**3.2.1 SMAHCs Without Pre-strained Wires.** In all of the results presented in the following, three different volume fractions of SMA wires as 4, 7 and 10% are considered. Figure 8 shows a diagram of average stress–strain of SMAHCs at ambient temperature and zero percent pre-strain. As depicted in Fig. 8, by increasing the volume fraction of SMA wires, the amount of stiffness reduction in the second stage was increased due to the martensite phase transformation of more SMA wires at this stage. Summary of stiffness variations is depicted in Table 3.

After unloading, the amount of residual strain in SMAHCs for 4, 7 and 10% embedded SMA wires is 0.0402, 0.0704 and 0.1003%, respectively. Thus, the amount of residual strain is gradually increased with the percent of SMA wire. Due to contraction of host composite during the unloading step, induced residual stress in SMA wires will be compressive. Figure 9 shows the stress–strain curve of a typical SMA wire inside the SMAHC laminate, contained 7% of SMA wires, under loading–unloading and loading steps.

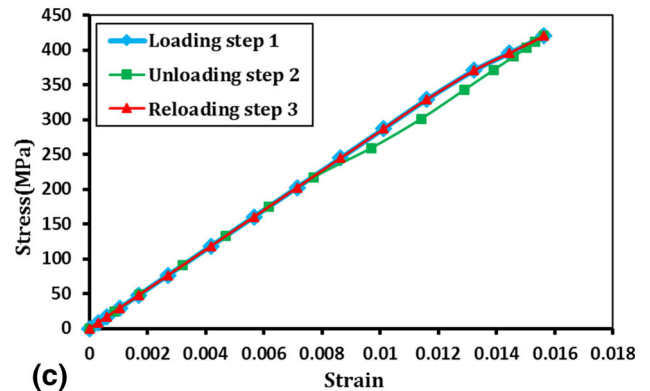
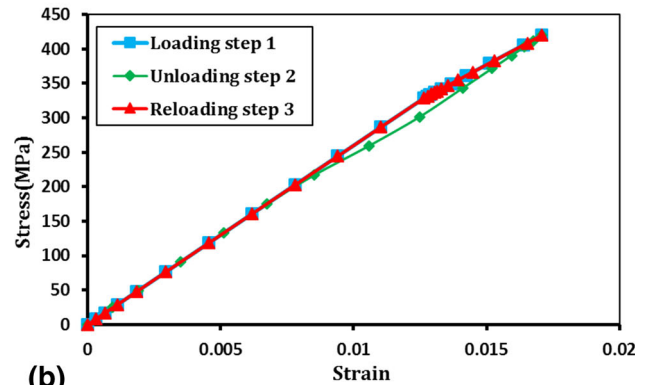
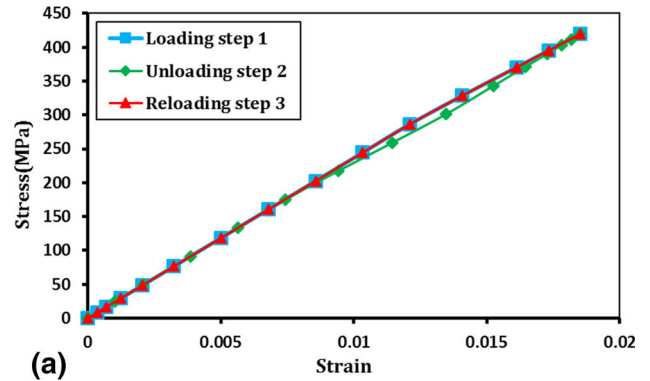


**Fig. 10** Average stress–strain behavior of SMAHCs at elevated temperature, containing SMA wires with volume fractions of (a) 4%, (b) 7% and (c) 10%

Figure 10 shows a diagram of average stress–strain of SMAHCs at elevated temperature and zero percent pre-strain. According to Fig. 10 at elevated temperatures, for prescribed wire volume fractions there is no residual strain in global stress–strain curves.

There is a remarkable difference between stress–strain curves predicted in the room and elevated temperatures during unloading phase. As depicted in Fig. 10, during unloading at elevated temperatures, SMA wires are following the curve shown in Fig. 11, so a stiffness reduction in global behavior happens which is dismissed by reducing the stress level and happening stress-induced phase transformation in SMA wires.

In addition, during the unloading step, some residual strain was observed in SMAHC specimens at ambient temperature, which was disappeared at elevated temperature. This is due to the superelastic performance of the SMA wires inside the SMAHC laminates at elevated temperature. The stress–strain curve of the SMA wire at elevated temperature is shown in Fig. 11 for the laminates with 7% of embedded SMA wires during loading–unloading and reloading steps.

Since the stress–strain behavior of host composite is assumed linear elastic during loading and unloading cycle at an elevated temperature no residual strain happened in the

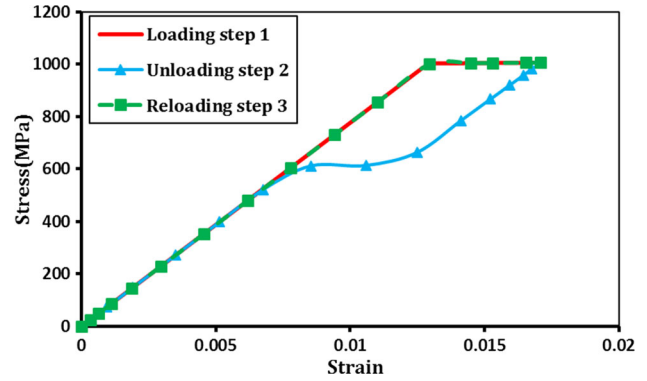
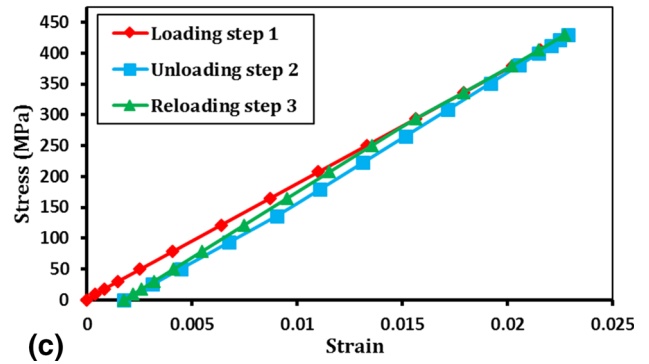
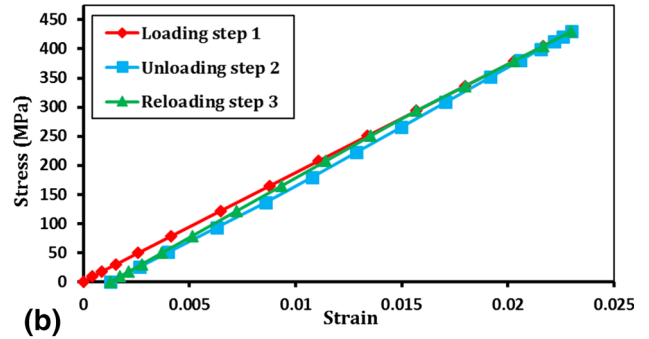
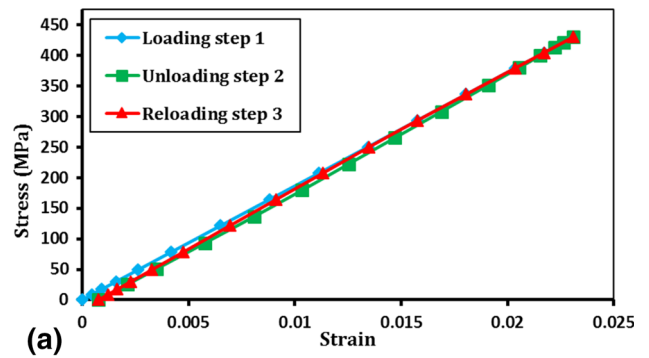


Fig. 11 Stress–strain response of SMA wire inside the SMAHC laminate at elevated temperature

Fig. 13 Average stress–strain behavior of SMAHCs at room temperature, containing 4% pre-strained SMA wires with volume fractions of (a) 4%, (b) 7% and (c) 10%

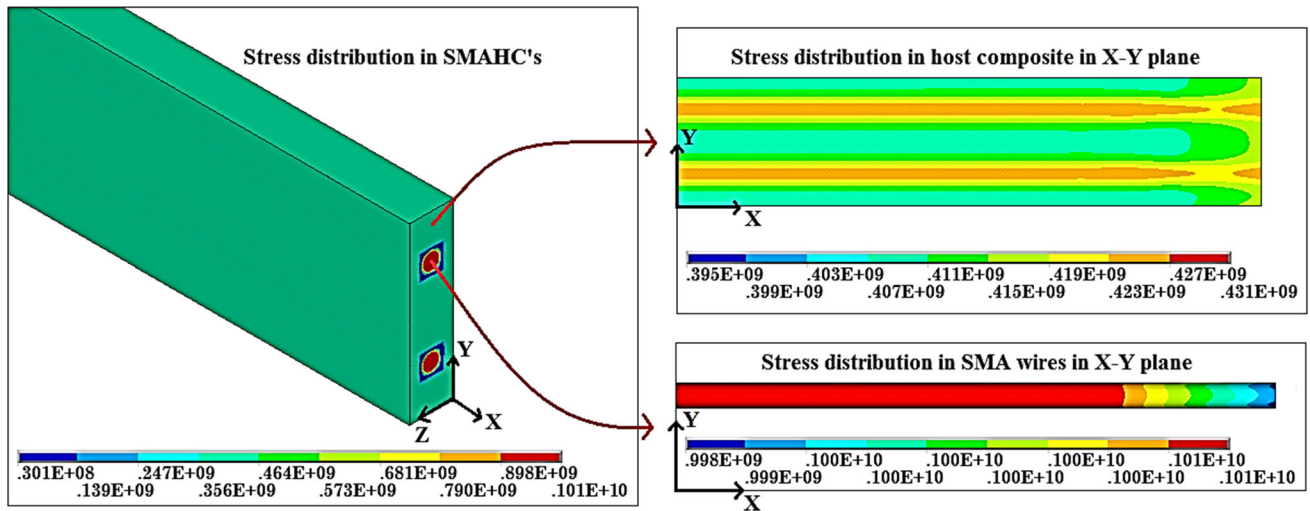


Fig. 12 Stress distribution in SMAHCs (left), SMA wires and the host composite (right) at elevated temperature



specimens. Worth to mention, in FE simulation specimens are loaded up to 80 percent of their experimental static strength.

The effects of SMA volume fraction on the effective modulus of hybrid composites estimated by simulations and ROM are compared in Table 3. As seen, at the first stage the effective modulus of SMAHC is steadily improved but in second stage there is a remarkable reduction due to the martensite transformation in SMA wires. Therefore, an optimized volume fraction of SMA wires should be considered to design optimal smart composite structures.

Stress distribution in SMAHCs, SMA wires and the host composite is depicted in Fig. 12 for the FE model containing 7% of SMA wire without pre-strain. Stress distribution became uniform at distances about width from the ends of the specimen. Uniform stress in SMA wires is around 1000 MPa which will cause stress-induced phase transformation from austenite to detwinned martensite in the wires.

**3.2.2 SMAHCs with Pre-strained Wires.** The average stress–strain curves for hybrid composites in ambient temperature are shown in Fig. 13. At the first stage of Fig. 13 (strain between 0 and 0.009%), effective modulus for hybrid composite with 4, 7 and 10% SMA wires, respectively, is 21.61, 22.39 and 23.21 GPa, and in the second stage, respectively, is 20.53, 20.55 and 20.58 GPa. As seen, effective modulus of the hybrid composite is less than host composite.

According to Fig. 13, the amount of residual strain in SMAHC specimens after unloading is more than specimens without pre-strain shown in Fig. 8. Effective modulus obtained by FE simulation and ROM is tabulated in Table 4 at ambient and elevated temperatures.

According to ROM at the second stage of Fig. 13, a reduction in the effective modulus was expected, while a small increase in the modulus is reported. This is due to the martensite transformation completion of SMA wires at 1.8% strain and entering to the stiff detwinned martensite phase. This increase in Young's modulus is shown in Fig. 13(c). At this point, Young's modulus was increased from 20.58 to 21.29 GPa. According to Fig. 13, the amount of residual strain of hybrid composites after unloading is 0.0764, 0.128, and 0.177%, for 4, 7 and 10% of SMA wires, respectively.

During loading of specimens with 4% pre-strain, SMA wires have experienced around 6% strain inside the host composite which could induce a large amount of compressive stress on the host composite during unloading. Figure 14 shows the amount of compressive stress on the hybrid composite to different percentages of the SMA wires.

As seen, by increasing the volume fraction of SMA wires, compressive stress on the host composite is increased.

According to Fig. 15, the behavior of hybrid composites with pre-strained SMA wires at elevated temperature is a bilinear curve. In this case, after unloading, a considerable amount of strain will be recovered in specimens. By using Eq 3 and 7, Young's modulus of SMA wires obtained is 53.78 GPa. Young's modulus variations of SMA wires as a function of strain due to the induced phase transformation stress are shown in Fig. 16. The effective modulus of SMAHC composites is improved by using SMA wires at elevated temperatures.

According to the presented results in Table 4, it is concluded that the overall stiffness of hybrid composites with pre-strained SMA wires is reduced at both temperatures.

In contrast to Fig. 10, during unloading of SMAHCs containing 4% of pre-strained wires, some residual strain would stay in the unloaded specimens. The amount of residual strain, as shown in Fig. 15, for different percentages of SMA wires is 0.0537, 0.0699, and 0.0831%, respectively. Energy dissipation and nonlinear loading and unloading stress–strain curves of SMAHCs with and without pre-strain could be explained by comparing Fig. 10 and 15. In addition, by comparing Fig. 11 and 17, it is concluded that specimens with pre-strain are a good candidate to dissipate energy by their hysteresis loop in comparison with specimens without pre-strain.

SMA wires in pre-strained specimens enter to phase transformation and modulus reduction at strains around 0.25%, while in specimens without pre-strain phase transformation start at strains around 1.28%. Also, loading and unloading cycle in pre-strained specimens caused the SMA

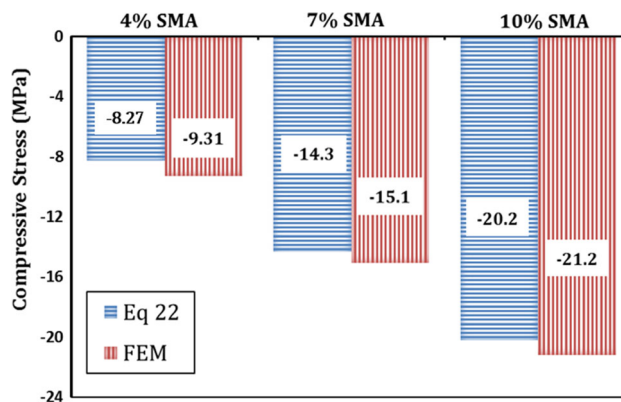
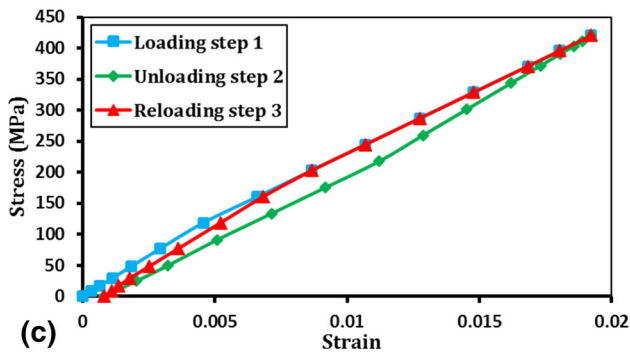
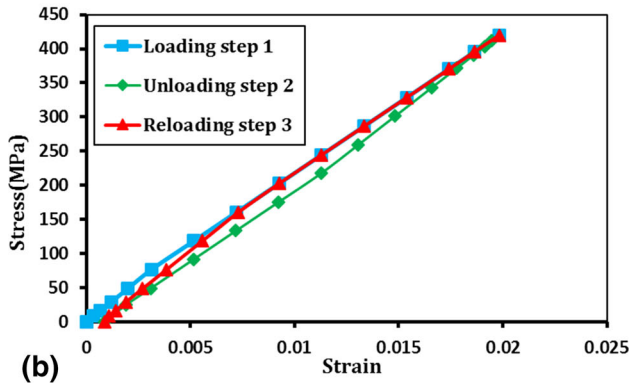
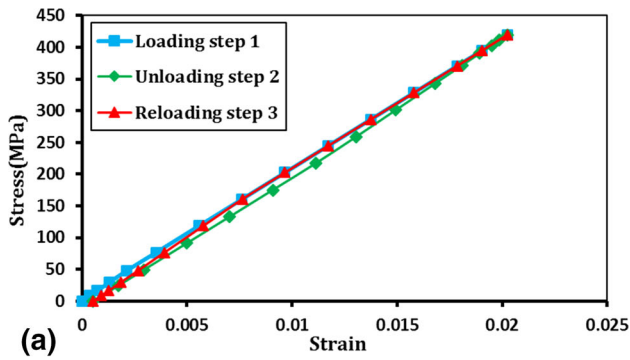


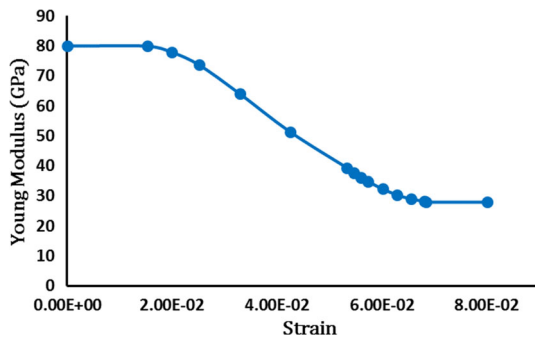
Fig. 14 Compressive stress on the composite after releasing the SMA wires at ambient temperature

Table 4 Effects of SMA volume fraction on the effective modulus of SMAHCs containing pre-strained SMA wires

SMA volume fraction	First stage			Second stage		
	4%	7%	10%	4%	7%	10%
Effective modulus, GPa						
Ambient temperature						
FEM	21.61	22.39	23.21	20.53	20.55	20.58
ROM (Eq 12)	21.55	22.33	23.11	20.47	20.44	20.41
Elevated temperature						
FEM	22.83	24.52	26.27	20.53	20.55	20.59
ROM (Eq 12)	22.58	24.14	25.69	20.47	20.44	20.41



**Fig. 15** Average stress–strain behavior of SMAHCs at elevated temperature, containing 4% pre-strained SMA wires with volume fractions of (a) 4%, (b) 7% and (c) 10%



**Fig. 16** Young's modulus of SMA wires vs. strain

wires to follow a loading–unloading path as shown in Fig. 17. Effective modulus obtained by FEM and ROM is tabulated in Table 4 at ambient and elevated temperatures.

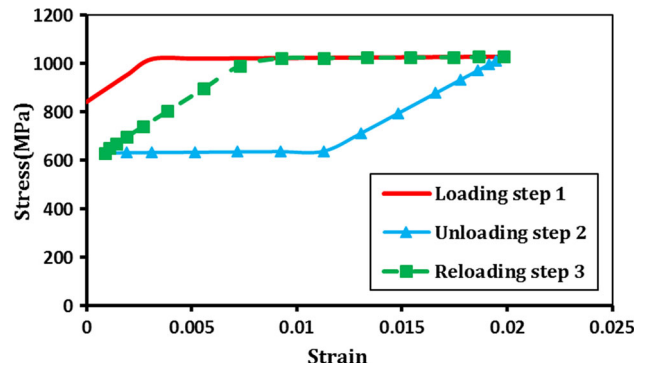


**Fig. 17** Stress–strain curve of SMA wire inside the SMAHC laminate at elevated temperature (wire volume fraction of 4% and pre-strain of 7%)

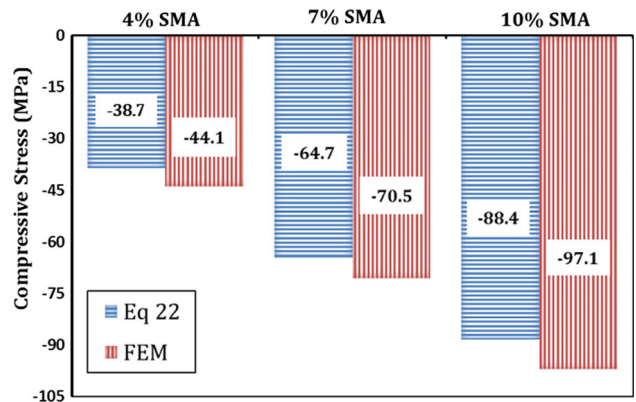


**Fig. 18** Compressive stress on the host composite after releasing the SMA wires at high temperature

As seen, at the first stage the effective modulus of SMAHCs is steadily improved but in the second stage, there is a remarkable reduction due to the martensite transformation in SMA wires.

Embedding the pre-strained SMA wires inside the laminated composite during fabrication and releasing them after composite solidification would cause a compressive stress on the host composite. The amount of induced compressive stress in the host composites is shown in Fig. 18. As seen, by increasing volume fraction of SMA wires the compressive stress was increased.

As seen in Fig. 14 and 18, the host composite compressive stress values calculated by Eq 22 and FE simulation are in good agreement. According to the presented discussion wires, volume fraction and pre-strains are two key points to control the final behavior of smart structures made of SMA wires and layered composites.

## 4. Conclusion

This study investigated the effect of embedding SMA wires on the macroscopic mechanical behavior of woven E-glass/epoxy composites subjected to uniaxial tensile loading through finite element simulations. Also, the effects of various parameters such as wires volume fraction, temperature and pre-strain were evaluated. At the first step, the accuracy of the FE

simulation was verified by using the experimental data available in the literature. Then the effects of various parameters were investigated by using FE models. According to the study conducted, the following observations are drawn:

- (a) Smart structures fabricated by using composite layers and pre-strained SMA wires at ambient and elevated temperatures will exhibit overall stiffness reduction which would be increased by adding SMA wires volume fraction.
- (b) Smart structures fabricated by using composite layers and SMA wires without pre-strain exhibited overall stiffness reduction at ambient temperatures. However, by increasing temperature, an improvement on the overall stiffness of SMAHCs is observed due to phase transformation of SMA wires from the martensite to the austenite phase.
- (c) The amounts of compressive stresses in hybrid composites at both temperatures were enhanced with the percentage of embedded SMA wires.
- (d) Energy dissipation by SMAHCs at elevated temperature with embedded pre-strained SMA wires was more than SMAHCs with SMA wires without pre-strain.
- (e) By comparing the results, this conclusion is made that application of SMA wires without pre-strain is better than pre-strained wires in terms of stiffness enhancement of the host composite, but in applications which strain recovery capabilities of SMA wires are important like crack mitigation pre-strained SMA wires are preferred.
- (f) Proposed 1-D model based on strength of materials is capable of predicting the induced residual strain in the host composite with acceptable correlation in comparison with available 3-D nonlinear model implemented in the commercial software.

## References

1. J. Aurrekoetxea, J. Zurbitu, I. Ortiz de Mendibil, A. Agirregomezkorta, M. Sánchez-Soto, and M. Sarrionandia, Effect of Superelastic Shape Memory Alloy Wires on the Impact Behavior of Carbon Fiber Reinforced In Situ Polymerized Poly(Butylene Terephthalate) Composites, *Mater. Lett.*, 2011, **65**, p 863–865
2. H.K. Cho and J. Rhee, Nonlinear Finite Element Analysis of Shape Memory Alloy (SMA) Wire Reinforced Hybrid Laminate Composite Shells, *Int. J. Non Linear Mech.*, 2012, **47**, p 672–678
3. Q.-Q. Ni, R. Zhang, T. Natsuki, and M. Iwamoto, Stiffness and Vibration Characteristics of SMA/ER3 Composites with Shape Memory Alloy Short Fibers, *Compos. Struct.*, 2007, **79**, p 501–507
4. F. Taheri-Behrooz, F. Taheri, and R. Hosseinzadeh, Characterization of a Shape Memory Alloy Hybrid Composite Plate Subject to Static Loading, *Mater. Des.*, 2011, **32**, p 2923–2933
5. E. Wongweerayoot, W. Srituravanich, and A. Pimpin, Fabrication and Characterization of Nitinol-Copper Shape Memory Alloy Bimorph Actuators, *J. Mater. Eng. Perform.*, 2015, **24**, p 635–643
6. Y. Xiao, P. Zeng, and L. Lei, Experimental Investigation on the Mechanical Instability of Superelastic NiTi Shape Memory Alloy, *J. Mater. Eng. Perform.*, 2016, **25**, p 3551–3557
7. X. Wang and G. Hu, Stress Transfer for a SMA Fiber Pulled Out from an Elastic Matrix and Related Bridging Effect, *Compos. Part A Appl. Sci. Manuf.*, 2005, **36**, p 1142–1151
8. H. Asadi, Y. Kiani, M. Shakeri, and M.R. Eslami, Exact Solution for Nonlinear Thermal Stability of Geometrically Imperfect Hybrid Laminated Composite Timoshenko Beams Embedded with SMA Fibers, *J. Eng. Mech.*, 2015, **141**, p 4014144
9. Z. Deng, Q. Li, A. Jiu, and L. Li, Behavior of Concrete Driven by Uniaxially Embedded Shape Memory Alloy Actuators, *J. Eng. Mech.*, 2003, **129**, p 697–703
10. K. Lau, W. Chan, S. Shi, and L. Zhou, Interfacial Bonding Behavior of Embedded SMA Wire in Smart Composites. Micro-scale Observation, *Mater. Des.*, 2002, **23**, p 265–270
11. Z. Su, H. Mai, M. Lu, and L. Ye, The Thermo-mechanical Behavior of Shape Memory Alloy Reinforced Composite Laminate (Ni-Ti/Glass-Fibre/Epoxy), *Compos. Struct.*, 1999, **47**, p 705–710
12. A. Shimamoto, H. Ohkawara, and F. Nogata, Enhancement of Mechanical Strength by Shape Memory Effect in TiNi Fiber-Reinforced Composites, *Eng. Fract. Mech.*, 2004, **71**, p 737–746
13. J. Lee and M. Taya, Strengthening Mechanism of Shape Memory Alloy Reinforced Metal Matrix Composite, *Scr. Mater.*, 2004, **51**, p 443–447
14. A.R. Damanpack, M.M. Aghdam, and M. Shakeri, Micro-mechanics of the Composite with SMA Fibers Embedded in the Metallic/Polymeric Matrix Under Off-Axial Loadings, *Eur. J. Mech. A Solids*, 2015, **49**, p 467–480
15. Y. Zhu and G. Dui, Effect of Fiber Shape on the Mechanical Behavior of Composite with Elastoplastic Matrix and SMA Reinforcement, *J. Mech. Behav. Biomed. Mater.*, 2009, **2**, p 454–459
16. J. Raghavan, T. Bartkiewicz, S. Boyko, M. Kupriyanov, N. Rajapakse, and B. Yu, Damping, Tensile, and Impact Properties of Superelastic Shape Memory Alloy (SMA) Fiber-Reinforced Polymer Composites, *Compos. Part B Eng.*, 2010, **41**, p 214–222
17. H. Lei, Z. Wang, B. Zhou, L. Tong, and X. Wang, Simulation and Analysis of Shape Memory Alloy Fiber Reinforced Composite Based on Cohesive Zone Model, *Mater. Des.*, 2012, **40**, p 138–147
18. H. Lei, Z. Wang, L. Tong, B. Zhou, and J. Fu, Experimental and Numerical Investigation on the Macroscopic Mechanical Behavior of Shape Memory Alloy Hybrid Composite with the Weak Interface, *Compos. Struct.*, 2013, **101**, p 301–312
19. C. Liang and C.A. Rogers, One-Dimensional Thermomechanical Constitutive Relations for Shape Memory Materials, *J. Intell. Mater. Syst. Struct.*, 1990, **1**, p 207–234
20. K. Tanaka, S. Kobayashi, and Y. Sato, Thermomechanics of Transformation Pseudoelasticity and Shape Memory Effect in Alloys, *Int. J. Plast.*, 1986, **2**, p 59–72
21. Y. Ivshin and T.J. Pence, A Thermomechanical Model for a One Variant Shape Memory Material, *J. Intell. Mater. Syst. Struct.*, 1994, **5**, p 455–473
22. L.C. Brinson, One-Dimensional Constitutive Behavior of Shape Memory Alloys: Thermomechanical Derivation with Non-constant Material Functions and Redefined Martensite Internal Variable, *J. Intell. Mater. Syst. Struct.*, 1993, **4**, p 229–242
23. J.G. Boyd and D.C. Lagoudas, A Thermodynamical Constitutive Model for Shape Memory Materials. Part I. The Monolithic Shape Memory Alloy, *Int. J. Plast.*, 1996, **12**, p 805–842
24. J.G. Boyd and D.C. Lagoudas, A Thermodynamical Constitutive Model for Shape Memory Materials. Part II. The SMA Composite Material, *Int. J. Plast.*, 1996, **12**, p 843–873
25. F. Auricchio and R.L. Taylor, Shape-Memory Alloys: Modeling and Numerical Simulations of the Finite-Strain Superelastic Behavior, *Comput. Methods Appl. Mech. Eng.*, 1997, **143**, p 175–194
26. J.S. Tomblin, J. McKenna, Y.C. Ng, and K.S. Raju, B-Basis Design Allowables for Epoxy-Based Prepreg, *Newport E-Glass Fabric 7781/NB-321*, 2001, 3-033051
27. F. Auricchio, A Robust Integration-Algorithm for a Finite-Strain Shape-Memory-Alloy Superelastic Model, *Int. J. Plast.*, 2001, **17**, p 971–990
28. F. Auricchio, R.L. Taylor, and J. Lubliner, Shape-Memory Alloys: Macro-modelling and Numerical Simulations of the Superelastic Behavior, *Comput. Methods Appl. Mech. Eng.*, 1997, **146**, p 281–312
29. A.C. Souza, E.N. Mamiya, and N. Zouain, Three-Dimensional Model for Solids Undergoing Stress-Induced Phase Transformations, *Eur. J. Mech. A Solids*, 1998, **17**, p 789–806
30. F. Auricchio and L. Petrinì, Improvements and Algorithmic Considerations on a Recent Three-Dimensional Model Describing Stress-Induced Solid Phase Transformations, *Int. J. Numer. Methods Eng.*, 2002, **55**, p 1255–1284
31. Anon in [www.memry.com](http://www.memry.com)